Nano Research
2022, 15(5): 4421–4430

ISSN 1998-0124 CN 11-5974/O4
https://doi.org/10.1007/s12274-021-4032-5

Research Article

Ultradurable, freeze-resistant, and healable MXene-based ionic gels for multi-functional electronic skin

Yao Lu[1], Xinyu Qu[1], Siying Wang[1], Ye Zhao[1], Yanfang Ren[2], Wenli Zhao[1], Qian Wang[1] (✉), Chencheng Sun[3] (✉), Wenjun Wang[2], and Xiaochen Dong[1] (✉)

[1] *Key Laboratory of Flexible Electronics (KLOFE) & Institute of Advanced Materials (IAM), School of Physical and Mathematical Sciences, Nanjing Tech University (NanjingTech), 30 South Puzhu Road, Nanjing 211816, China*
[2] *School of Physical Science and Information Technology, Liaocheng University, Liaocheng 252059, China*
[3] *School of Electronic and Information Engineering, Changshu Institute of Technology, Changshu 215500, China*

© Tsinghua University Press and Springer-Verlag GmbH Germany, part of Springer Nature 2021

Received: 7 October 2021 / **Revised:** 10 November 2021 / **Accepted:** 21 November 2021

ABSTRACT

Hydrogel is a potential matrix material of electronic-skins (E-skins) because of its excellent ductility, tunability, and biocompatibility. However, hydrogel-based E-Skins will inevitably lose their sensing performance in practical applications for water loss, physical damage, and ambient interferences. It remains a challenge to manufacture highly durable gel-based E-skins. Herein, an E-Skin is fabricated by introducing ionic liquids (ILs) into MXene-composited binary polymer network. The obtained ionic gel shows excellent mechanical properties, strong adhesion, and superior tolerance to harsh environments. The E-skin exhibits high sensitivity to both strain and pressure in a wide range of deformations, which enables a monitoring function for various human motions and physiological activities. Importantly, the E-skin shows consistent electrical response after being stored in the open air for 30 days and can be quickly healed by irradiation with 808 nm near-infrared light, originating from the photo-thermal effect induced self-healing acceleration. It is noteworthy that the E-skin also reveals a highly sensitive perception of temperature and near-infrared light, displaying the promising potential applications in the multifunctional flexible sensor.

KEYWORDS

E-skins, MXene, environment resistance, photothermal effect, flexible sensor

1 Introduction

Human skin, the largest sensory organ in the human body to bridge various external stimuli from surroundings, has motivated numerous inspirations in flexible electronics. Electronic skins (E-skins), which mimic the sensory capability and flexibility of human skin, show a particularly broad application in human-machine interaction, decentralized healthcare service, and industrial robots [1–3]. It perceives, analyzes, and transmits multi stimuli, such as strain, pressure, temperature, and humidity, into visual electrical signals for signal acquisition and feedbacks in real-time [4–6]. Hydrogel, a three-dimensional (3D) cross-linked polymer network with high similarity to natural soft tissue, displays excellent ductility and biocompatibility to be a promising candidate in E-skin [7–10]. Specifically, how to meet sorts of rigorous requirements on stretchability, sensitivity, and multimodality of the hydrogel-based E-skins at various harsh environments are still under urgent demand.

The feasibility of hydrogel-based E-skins is severely restricted by the ambient environment and external interference. Ascribed to the high freezing point and saturated vapor pressure in the water, hydrogel-based E-skins are easily dehydrated to bring down the perception performance and durability of the E-skins, which also makes them not applicable at extreme temperatures [11–13]. Generally, with an elaborate encapsulation process on hydrogel electronic devices, the burden on dehydration and working temperature range can be greatly relieved. However, more complicated fabrication techniques and integration methods are required, which are not scalable for mass production. Therefore, many approaches have been proposed to endow hydrogels with negligible dehydration under a wide temperature range. The most commonly followed strategy is to introduce organic solvents, such as glycol, glycerol, sorbitol, or their mixtures, to reduce the crystallization point of the hydrogel [14–16]. For example, Li et al. prepared a glycerin-water mixed solvent hydrogel through a solvent exchange process [17]. The obtained gel-based sensor performed significant electrical sensitivity in a wide temperature range of −40–25 °C, which could meet the requirements of a variety of complex application environments. However, the poor biocompatibility and low conductivity of organohydrogels greatly limit their applications in biomedical and electrochemical devices. Recently, ionic liquids (ILs), as a cluster of organic ionic salt, have received extensive attention because of their excellent thermal stability, high conductivity, and fluidity at room temperature [18, 19]. Specifically, ILs are also identified as promising candidates of solvents in gel-based E-skins for a wide operating temperature range, low saturated vapor pressure, and high ionic conductivity than conventional water or organic solvents [20–22]. Moreover, the migration rates of ions in ILs vary at different operating temperatures, which paves the way for constructing multimodal perceived flexible sensors [23–25].

Address correspondence to Qian Wang, chelseawq@njtech.edu.cn; Chencheng Sun, ccsun@cslg.edu.cn; Xiaochen Dong, iamxcdong@njtech.edu.cn

In practical applications, the unexpected external force of friction and collision, and excessive stress under shear, twist, or stretch could damage the integrity of the gel, deteriorate its sensing performance and depress the durability and reliability of the gel-based E-skins. Therefore, it is of great significance to introduce self-healing properties into gel-based E-skins to prevent mechanical failure and prolong its service life [26, 27]. The self-healing ability is in close correlation to the reversible bonding in the polymer network. Researchers have proposed extensive studies on polymeric molecular design or device configuration to endow spontaneous repair with high self-healing efficiency [28–30]. There also have been a few attempts to facilitate the reorganization of reversible interaction under stimuli of heat, light, sound, or electricity [31]. Typically, the thermal activation presents a significantly enhanced self-healing rate through accelerating molecular thermal motion or reducing the activation energy for specific chemical reactions, but conventional direct heating is quite inconvenient and not applicable in most practical scenarios. Methods are under urgent demand to realize rapid self-healing with easy-accessible external stimuli, especially stimuli existing in the natural world. $Ti_3C_2T_x$, a typically used two-dimensional conductive filler in E-skins [32–34], is also protruded as a burgeoning photo-thermal reagent for its excellent electromagnetic absorption and thermal generation capability, which has flourished in energy storage and biomedical engineering [35–37]. It can absorb near-infrared light in a wide range of wavelengths with high photothermal conversion efficiency [38]. Therefore, the wounded part in MXene composited hydrogel can be healed accurately by laser irradiation at a pre-determined position to reach a high penetration depth within a short time, which is conducive to realizing rapid self-healing with high efficiency.

Herein, a durable ionic gel (PAA/CNC@TA/MXene, PCM) with approved mechanical property, high self-healing performance, and fatigue resistance was put forward by introducing ILs into a binary polymer network. Notably, the ionic gel showed an ultra-wide temperature using range (about –50–80 °C) and excellent durability to maintain its perceiving performance after being stored for 30 days in the air. The ionic gel-based E-skins exhibited high sensitivity toward a wide range of strain (0–270%) and pressure (0–60 kPa), and it could be applied to monitor various subtle and dramatic human movements to realize motion perception. Collaborate with the excellent photo-thermal effect of MXene, the ionic gel could also be proposed with optical sensing and feature an accelerated self-healing for photo-thermal conversion.

2 Experimental

2.1 Materials

Acrylic acid (AA, 98%), 1-ethyl-3-methylimidazolium ethyl sulfate (98%), N,N'-methylene bisacrylamide (MBA, 99%), ammonium persulfate (aps), α-cellulose, glycerite (99%), tris(hydroxymethyl)aminomethane (99%), lithium fluoride (99%) and tetramethylammonium hydroxide solution (TMAOH 25 wt.% in water) were purchased from Admas Co. Ti_3AlC_2 powder was purchased from Beijing Forsman Scientific (China). All the chemicals were used directly without further purification.

2.2 Synthesis of MXene nanosheets

MXene was prepared via an etching method based on previous literature [39]. Briefly, 1.0 g Ti_3AlC_2 powder and 1.0 g LiF were dissolved in 10 mL HCl solution (9 M). Afterward, the mixture was sealed in an oven at 200 °C for 24 h. Then, the obtained suspension was collected and washed by ultrapure water until a neutral solution was achieved. After dispersing the sediment in 10 mL TMAOH solution, Ti_3C_2 was collected after further centrifugation at 3,500 rpm and washing. Eventually, Ti_3C_2 nanosheets powders were obtained after drying the supernatant with a freeze-drying method.

2.3 Synthesis of cellulose nanocrystals CNC and CNC@TA

15 g α-cellulose and 150 mL H_2SO_4 solution (60 wt.%) were stirred in deionized (DI) water at 45 °C, and then 1.2 L DI water was added to terminate the reaction. Subsequently, the supernatant was washed repeatedly by DI water and centrifuged until pH was greater than 8.5. After dialysis for 5 days, the suspension was freeze-dried to obtain CNC powder. Thereafter, an equal mole of TA was added into 10 wt.% CNC solution and stirred for 6 h. Tris(hydroxymethyl)aminomethane buffer solution was added to adjust the pH to 8. After another stirring for 3 h, the acquired brown mixed solution was centrifuged at 7,000 rpm and the supernatant was freeze-dried to obtain CNC@TA.

2.4 Preparation and characterization of PCM ionic hydrogel

Firstly, 0.6 g acrylic acid and 2.1 g ILs were mixed, and a certain amount of CNC@TA and Borax solution was added. The mixed solution was divided into two parts, MXene nanosheets and MBA/APS were added, respectively. Remix the two solutions and put them into a 60 °C oven for 6 h, and PCM ionic gel was acquired. For comparison, the ionic gel without MXene was prepared and denoted as PC ionic gel. The control groups for different solutions of hydrogel and organohydrogel were obtained with the same methods, in which the ILs were replaced into water or glycerin/water (1:1) mixture. The conductivity of the three kinds of gels was evaluated through a linear voltammetry scanning method on an Electrochemical Workstation (Chenhua CHI660E, Shanghai) consecutive five times presented in our previous research [8]. To prevent water evaporation in the hydrogel/organohydrogel, the heating time of the reaction for the preparation of these gels was restricted to 0.5–1 h. The gels were stored at −50, −20, and 25 °C for 12 h, respectively, to evaluate the stretchability and durability intuitively in harsh environments.

2.5 Adhesion property characterizations

The adhesive strength of the gel was measured through a stripping method. Typically, one end of the gel was connected to the stretching platform of the caliper, and the other end adhered to the smooth surface of substrates. Different substrates were settled for adhesion evaluation. Three repeated adhesive strip tests were conducted, and the adhesive strength was calculated by average maximum tensile force divided by the original bonded area.

2.6 Weight loss measurements

Circular samples (Φ20 mm × 15 mm) were placed in an ambient environment (25 ± 2 °C, RH = 60%) for different periods at different temperatures. The mass-loss rate (Q) can be calculated by Eq. (1)

$$Q(\%) = \frac{W_t - W_0}{W_0} \times 100\% \quad (1)$$

where W_0 is the weight of the hydrogel before the dehydration experiment, W_t is the weight after the dehydration experiment.

2.7 Mechanical/electrical performance characterization

The mechanical performances of the gels were characterized on a mechanical testing apparatus (ESM302, Mark-10) at room

temperature (20 ± 2 °C). For the tensile tests, the gels were cut into regular strips of 30 mm × 3 mm × 2 mm and clamped to the two ends of the stretching machine, the tensile rate was set to be 60 mm·min^{-1}. Tensile strength and elongation at break were determined by the breaking point. For the pressure sensor, a specific cylindrical hydrogel with a diameter of 14 mm and a height of 8 mm was assembled, Cu foil was adhered to at each end of the cylinder and treated as the current collector. The resistance variations of the gels were detected by a semiconductor characterization system (Keithley 4200-SCS). The gel was secured to the mechanical testing apparatus to sustain different forms of mechanical deformations, each end of the gel was inserted with copper wires to connect to the Keithley 4200-SCS and the resistance changes were recorded. For human body movements monitoring and smartboard perception, the gel was completely encapsulated by electrodes and VHB tape and taped to the appropriate position.

2.8 Thermal-sensitive performance characterization

Seal a certain size of PCM ionic gel (2 cm × 1 cm × 1 cm) into a ziplock bag and place it in an oil bath to adjust the gel temperature. Connect conductors were drawn from each end of the ionic gel and connected to the Keithley 4200-SCS to acquire real-time resistance. The temperature of the gel varied with the settled bath temperature and the resistance changes were recorded. During the test, the ambient temperature was 18 ± 2 °C, and the temperature of the gel ranged from 20 to 90 °C.

2.9 Photothermal performance and optical response characterization

Ultraviolet absorption spectroscopy (Shimadzu UV-3600 UV–Vis Spectrophotometer) was used to evaluate the absorption of the gel in the near-infrared characteristic bands. Gels prepared with different contents of MXene nanosheets were cut into cubes (10 mm × 5 mm × 2 mm) and placed directly below the laser emitter at a distance of 3 cm from the laser emission point to the gel surface. Afterward, the gel was irradiated under an 808 nm laser for a certain period at different power densities. Conductors were fixed at the opposite surface of the cube and connected to the Keithley 4200-SCS to display the changes of current under irradiation, an infrared camera (FLIR, Arlington, VA) was used to reveal the real-time temperature changes of the ionic gels during the irradiation process.

2.10 Self-healing performance

A piece of PCM ionic gel was cut into two pieces and re-contacted barely or under light irradiation. After different periods of healing time, the reconnected gel was stretched on the mechanical testing apparatus at a stretching rate of 60 mm·min^{-1}. The self-healing efficiency (η) can be calculated by Eq. (2)

$$\eta(\%) = \frac{\varepsilon}{\varepsilon_0} \times 100\% \quad (2)$$

Where ε is the elongation at break after self-healing and ε_0 is the original elongation at break. To evaluate the electrical network reconstruction of the PCM ionic gel, both ends of the gel were connected to the Keithley 4200-SCS and the resistance of the gel at 1 V bias voltage was measured. To detailed demonstrate the microstructure evolution of incision during the self-healing period, a Nikon microscope (magnification 50) was utilized to record the profiles of the gel surface in real-time.

3 Results and discussion

3.1 Materials synthesis

Most biological soft tissues, such as ligaments and cartilage, are composed of soft and hard interactive structures, the synergistic effect of the "hard" and "soft" components enables biological tissues high deformability, toughness, rapid and sensitive perception to external forces [40, 41]. For example, tendons, formed by soft connective tissue connected with rigid collagen fibers, are capable of withstanding thousands of deformations. Inspired by these biological soft tissues, the multiple perceived highly conductive and mechanical robust ionic gels with "hard and soft cooperation" -- PCM ionic gel was prepared through a one-step thermal-polymerization method. Figure 1 schematically demonstrates the composition and extensive physical and chemical interactions in the PCM ionic gel.

In the two-blocked polymer matrix, the chemical crosslinked poly(acrylic acid) (PAA) network is soft and brittle. And, the tough CNC@TA nanorods were added to anchor the polymer long chains and enhance the gel's mechanical property. Uniform and stable CNC@TA nanorods were prepared by a representative coating method [42]. The Fourier-transform infrared spectroscopy spectra of CNC@TA presents notable stretching peaks in contrast to unmodified CNCs, including a peak at 1,713 cm^{-1} from

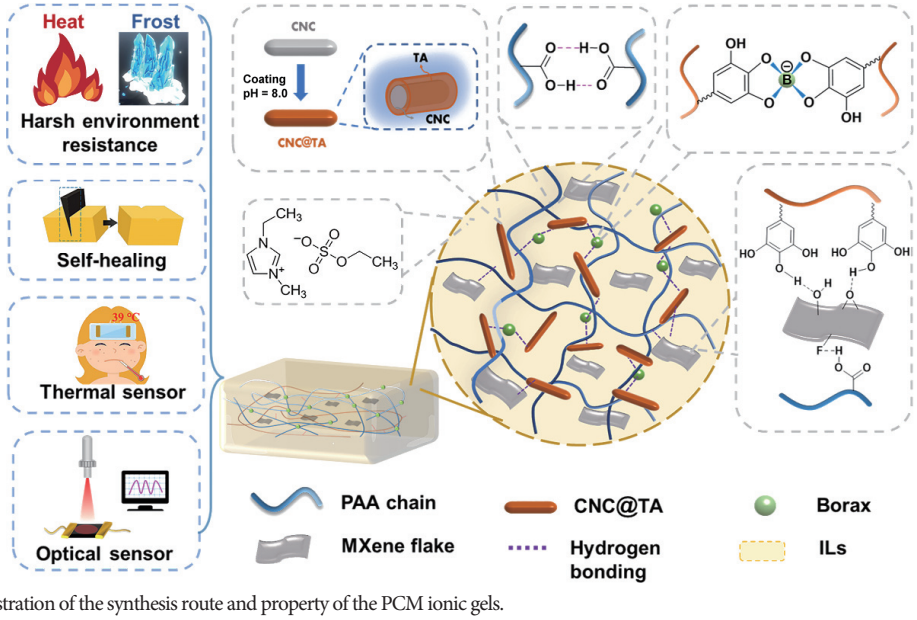

Figure 1 Schematic illustration of the synthesis route and property of the PCM ionic gels.

stretching vibration of COO– and another featured peak at 1,451 cm^{-1} from distortion vibrations of C=C in the benzene rings (Fig. S1(a) in the Electronic Supplementary Material (ESM)). Atomic force microscope (AFM) images also manifest distinct dimensional variation of the nanorods after TA coating (Figs. S1(b) and S1(c) in the ESM). In addition, a large number of phenolic hydroxyl groups on TA form extensive hydrogen bonds with PAA, MXene, or each other, as well as borate-diol dynamic complex bonds with free boric ions, generating a highly crosslinked polymer matrix. Specifically, the synergistic effect of the two categories, the strong interaction of borate-diol bonds and weak sacrifice bond of hydrogen bonds, can promote rapid energy conduction and dissipation and effective recombination of polymer chains under external stimuli, showing enhanced mechanical toughness and excellent self-healing property in the ionic gel [43].

Furthermore, MXene is mixed into ionic liquid (1-ethyl-3-methylimidazolium dicyanamide) to form indispensable interaction with the polymer network through abundant surface functional groups. MXene nanosheets were prepared by an improved wet etching method, which has been revealed in our previous work [44]. Figure S2(a) in the ESM demonstrates the X-ray diffraction (XRD) patterns of the MAX phase and the resulted MXene nanosheets. The characteristic peak of MAX at 9.5° shifts to a lower degree of 4.8° in MXene, which is consistent with the (002) plane of $Ti_3C_2T_x$. The transmission electron microscopy (TEM) image also presents a sketch of the large and ultra-thin MXene nanosheets (Fig. S2(b) in the ESM). Together with the ILs, MXene nanosheets are evenly dispersed into the gel and establish a three-dimensional conductive network in the gel, showing high sensitivity for intellisense.

3.2 Mechanical performance characterization

The CNC@TA nanorods propose indispensable “hard” segments in the polymer matrix and establish strong interaction with the MXene composited ionic gel, showing an unpredictable impact on the mechanical performance. As shown in Fig. 2(a), the stress-strain curves of the ionic gels show complicated evolutionary trends with different contents of CNC@TA. It appears that the ionic gel with 1 wt.% content of CNC@TA displays the optimum balanced mechanical property, demonstrating an improved elongation at break and fracture strength of 1,300% and 100.4 kPa compared to PAA ionic gel (425%, 30.4 kPa). The principles of mechanical enhancement originate from the “tendon-like” polymer heterostructure. Under the external stimuli, the weaker "soft segment" can effectively transfer stress to the "hard segment" to alleviate mechanical damage. On the other hand, the extensive inter-chain hydrogen bonds between the polymer networks and CNC@TA nanorods sustain rapid breaking and recombination with the slip of nanorods, which can dissipate energy efficiently and avoid fracture deformation to reveal optimized mechanical strength.

Figure 2(b) shows that both the elongation at break and the strength of the gel are improved (1,470%, 135.2 kPa) after the MXene addition. Figure S3 in the ESM shows the stress-strain curves of consecutive five tension-release cycles with 140% strain. After the inevitable deterioration of properties during the first cycle for the viscosity of matrix and the fracture of some permanent chemical bonds, PCM ionic gel in the subsequent tensile cycle can effectively recombine the dynamic reversible bonds and shows distinguished resilience. Moreover, the obtained PCM ionic gels are highly deformable to be twisted, knotted, and stretched after knotting, it also presents a strong toughness to hold up a 200g weight without fracture (Fig. 2(c)). With sufficient non-covalent bonds in the polymer network, such as hydrogen bonding and metal complexation, PCM ionic gels display strong adhesion to various smooth substrates of plastic, wood, rubber, and metal (Fig. 2(d)). In addition, the ionic gels also characterize tough adhesion to the bone imitating material PTFE, suggesting a promising candidate for bone tissue regeneration. Moreover, as shown in Fig. 2(e), the ionic gels can directly attach to human fingers to undertake deformations of bending and stretching without residue after being removed, which is conducive to avoiding severe inflammation or allergies and extending its application in biological dressings.

3.3 Harsh environment tolerant measurement

In practice, flexible electronics would inevitable exposure to various harsh conditions, such as a wide range of temperature or humidity, while it remains a challenge to fabricate a highly durable gel to meet diverse critical requirements. To explore the superiority of ILs in harsh conditions, the properties of gels with different solutions are evaluated, where DI water and glycerin-water (1:1) composite were adopted to prepare hydrogels and organohydrogels, respectively. The three gels were stored at –50, –20, and 25 °C for 12 h, respectively. As shown in Fig. 3(a), the hydrogel becomes hard and brittle after being stored at subzero temperature and breaks under a tiny stretch, while the organohydrogel maintains mechanical extensibility at –20 °C because of the ice crystallization inhibition after glycerol

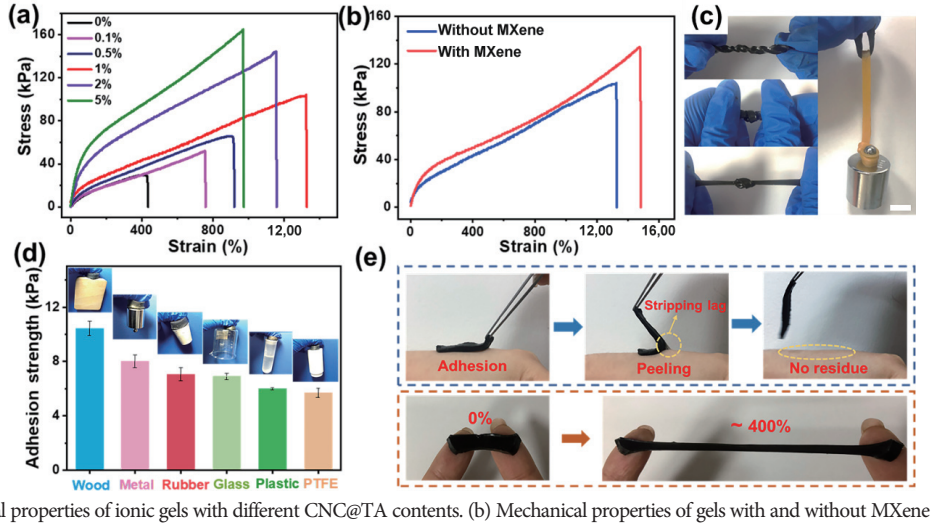

Figure 2 (a) Mechanical properties of ionic gels with different CNC@TA contents. (b) Mechanical properties of gels with and without MXene (1 wt.% CNC@TA). (c) Photos of mechanical properties (scale: 1 cm). (d) and (e) Comparison of adhesion properties of gels with different materials and photos of adhesion.

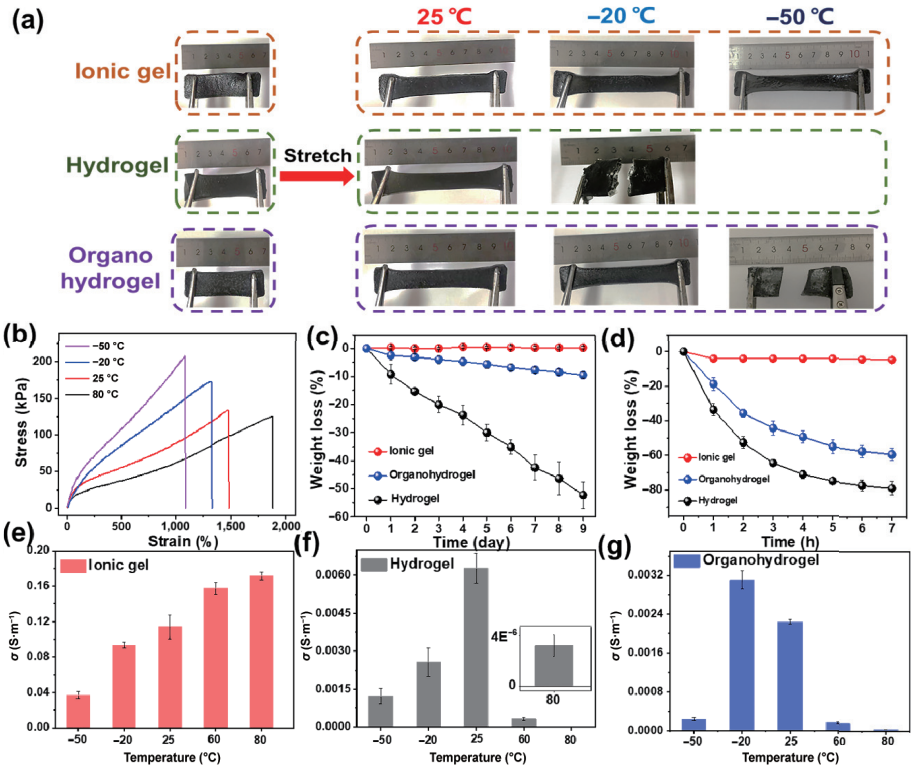

Figure 3 (a) Tensile performance of ionic gel, hydrogel, and organohydrogel after storage at –50, –20, and 20 °C. (b) Tensile curves of PCM ionic gels after being stored at different temperatures. The solution retention ability of PCM ionic gel, hydrogel, and organohydrogel being stored at (c) 25 and (d) 80 °C. (e)–(g) The conductivity of PCM ionic gel, hydrogel, organohydrogel after being stored at different temperatures.

compositing. When the storage temperature drops to –50 °C, the ice crystals precipitate and frost on the surface of the gel. The organohydrogel fails its elasticity and destructs when subjected to about 80% tension. It is worth noting that the ionic gels display satisfying stretchability after storage both at –50 and –20 °C. This phenomenon may be coming from the particularly low crystallization point of the ILs (Fig. S4 in the ESM), which ensures the usability of the gel after subzero temperature storage and confirms the wide temperature applicability of the PCM ionic gel.

Tensile tests of PCM ionic gels after being stored at –50, –20, 25, and 80 °C are presented in Fig. 3(b). With the storage temperature decrease, the elongations at break descend while the tensile strengths are enhanced for the limited movement of polymer chains at low temperatures. It is noteworthy that PCM ionic gels reach superior stretchability of more than 1,000% in the whole temperature range of –50–80 °C, which underlines a wide temperature range of the gel-based E-skin. Figure 3(c) shows the water retention ability of three gels during the 10 days storage at 25 °C and 60% RH. Compared to the hydrogel and organohydrogel, which lose 53% and 14% of theirs' original weight, the weight of PCM ionic gel remains constant throughout the testing process, suggesting the predominant durability and reliability of the ionic gel after long time storage at room temperature. The durability of three kinds of gels is further characterized at 80 °C for 7 h. Figure 3(d) reveals that the hydrogel and organohydrogel suffer from violent water evaporation and badly damage at high temperatures, while PCM ionic gel maintains negligible weight loss and finally loses 5.7% of its initial weight without changing its shape, demonstrating its wide temperature range of applicability. The inevitable weight loss might be attributed to the initially absorbed moisture.

To explore the feasibility of the ionic gel at different temperatures, the ionic conductivity of three gels is measured and compared in Figs. 3(e) and 3(f). The conductivity of ionic gels is about 0.12 S·m^{-1} at 25 °C, nearly two orders of magnitude higher than that of hydrogel and organohydrogel. The migration rate of charge carriers is in close correlation with temperature. In consequence, the conductivity of ionic gels demonstrates a distinctly rising trend with the temperature increase in the range of –50 to 80 °C in Fig. 3(e). Contrary to PCM ionic gel, the conductivities of hydrogel and organohydrogel do not show apparent temperature dependence. In particular, attributed to the violent water loss at high temperatures (60 and 80 °C), a sharp decrease of conductivity is emerged in hydrogels and organohydrogel, which evidences that those two gels are not suitable for high-temperature applications.

3.4 Electrical performance characterization

A typical strain sensor is presented to determine the electromechanical performance of PCM ionic gel. As shown in Fig. 4(a), the PC ionic gel (ionic gel without MXene) displays an approximately linear resistance response to the tensile, which is attributed to the ionic transfer of ILs in the gel under constant applied voltage. Gauge factor (GF), the fundamental indicator to evaluate the sensitivity of the strain sensor, is calculated from the formula GF = $(\Delta R/R_0)/\varepsilon$ to be 0.44, where R_0 is the initial resistance, ΔR is the relative resistance variation, and ε is the applied strain. In contrast, the sensing performance of the PCM ionic gel is greatly enhanced after compositing 1.0 wt.% MXene nanosheets. Ascribed to the synergistic effect of electron conduction and ion transfer in PCM ionic gel, GF increases to 1.04 in the strain range of 0–170% and rises further to 2.61 in the range of 170%–270%. It is supposed that the jointed MXene nanosheets move and slip under strain deformations, and the consequent irregular changes in conductive path ultimately carry out an enhanced sensing performance [45, 46].

Figure 4(b) shows the relative resistance change of the strain sensor at strains ranging from 20% to 180%. The consecutive three cycles keep identical at fixed strain and demonstrate distinct discrepancies for different strains, indicating that the strain sensor can monitor different degrees of tensile strain with high reliability.

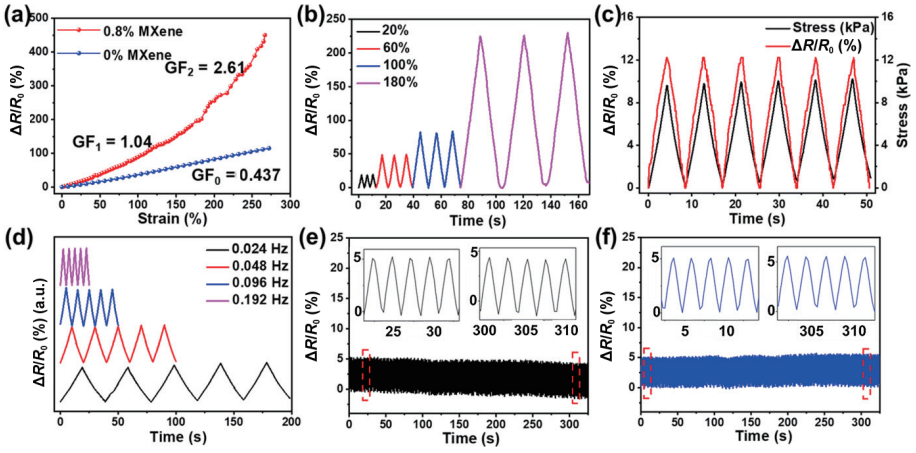

Figure 4 Electrical performances of PCM ionic gel-based strain sensors. (a) The relative resistance changes of PC ionic gel and PCM ionic gel within the 270% strain range. (b) The electrical response under strains of 20%, 60%, 100%, and 180%. (c) Electromechanical hysteresis. (d) Cyclic stretching-releasing with different stretch frequencies. (e) and (f) Cyclic electrical response of ionic gels before and after 30 days storage (20 ± 2 °C).

Figure 4(c) compares the output relative resistance change waveform with the input stress at 15% strain. The responsive resistance variation waveforms are almost synchronous to the applied strain, affirming the negligible electromechanical hysteresis in the ionic gel-based strain sensor. As shown in Fig. 4(d), the relative resistance changes of the strain sensor with frequencies ranging from 0.048 to 0.186 Hz (under 50% strain) are repeatable and persistent, showing predominant frequency-dependent features to apply to different modes of movement monitoring. In addition, the strain sensor performs a brief response time of 156 ms and an approximate recovery time of 157 ms under a subtle stretch, ensuring a rapid response to an immediate stimulus of human motion (Fig. S5(a) in the ESM). Figure S5(b) in the ESM shows the relative resistance change of the strain sensor during repeated stretching and releasing cycles at 0–25% strain for 370 times. The relative resistance change is nearly constant throughout the durability test, showing high stability and reproducibility of the strain sensor. In addition, the baseline of the relative resistance variation manifests a declined trend during the cycling, which might be attributed to the environmental disturbance. Figure S6 in the ESM compares the relative resistance changes of the sensor at different temperatures and evidence of the possible temperature interference. Furthermore, the durability of the strain sensor is further characterized by evaluating the sensing performance after storage at 25 °C and 60% RH for 30 days. In Figs. 4(e) and 4(f), consecutive stretching-releasing cycles at 5% strain before and after storage are compared. The strain sensor exhibits substantially constant $\Delta R/R_0$ after 30 day's storage, demonstrating the ultra-durable sensing performance of the strain sensor, which is of great significance to the long-term practical application of PCM ionic gel-based strain sensor.

Meanwhile, with stacked conductive MXene nanosheets and an ion-conductive network, the PCM ionic gel also can be identified as a typical pressure sensor. Herein, a piece of cylindrical PCM ionic gel (Φ14 mm × 8 mm) is assembled into a pressure sensor, and the piezoresistive properties of the pressure sensor are exhibited (Fig. S7 in the ESM). The sensitivity of the pressure sensor is calculated to be 1.54 kPa^{-1} in the range of 0–26 kPa and 0.72 kPa^{-1} in the range of 26–60 kPa (Fig. S7(a) in the ESM). The pressure sensor also reveals distinct relative current changes under different pressure of 0.5, 2, and 12 kPa under successive three cycles (Fig. S7(b) in the ESM). The pressure sensor also reveals a rapid response rate with a response time of 125 ms under small compression and 117 ms for recovery (Fig. S7(c) in the ESM). In addition, the pressure sensor displays highly durable and reproductive electrical perception to cyclic pressure load of 7.0 kPa 400 times (Fig. S7(d) in the ESM). Conclusively, the PCM ionic gel-based pressure sensor is labeled with high sensitivity in a relatively wide sensing range, rapid response rate, and superior stability, being a promising candidate for flexible wearable devices.

3.5 Human motion detections and handwriting test

With brilliant sensing performance to both strains and pressures, PCM ionic gel sensor shows a wide prospect to adhere to various human body surfaces to carry out full ranges of human motion detections. In Fig. 5(a), the flexible sensor is settled at the knee and the relative current shows a sharp rising response to the leg lifting. Figure 5(b) shows the perception current evolution when adhered at the joint to monitor finger bending. When the finger bends at a certain angle (45° and 90°), the relative current changes display instant fluctuations, and the waveforms are more distinct with a higher bending angle. With the sensor is attached near the mouth (Fig. 5(c)), the relative current shows a significant ascent or descent at smiling or crying. The distinct electrical signals are originated from the differentiable jaw muscles moving trends, which prospect the sensor in the field of facial expression recognition. The flexible sensor can also be assembled into a smart "writing board", as profiled in Fig. 5(d). With different writing directions, strengths and speeds, the current signals show featured shapes of peaks in writing different Arabic numbers (Fig. 5(e)). The accurate detection of handwriting demonstrates the great potential of PCM ionic gel-based sensors for intelligent input and handwriting identification.

3.6 Temperature response perception

ILs are composed of two positively and negatively charged molecules, displaying unique physical and chemical characteristics [18–23]. In particular, with the increase of temperature, the dissociation of ion pairs is greatly activated and the number and migration rate of carriers is enhanced thereafter, showing distinct improvement in conductivity (Fig. 6(a)). Figure 3(e) has evidenced the monotone increase of conductivity to temperatures and inspired the exploration of PCM ionic gel on temperature perception. As shown in Fig. 6(b), the relative current variations of PCM ionic gel increase almost linearly with the gradual increase of temperature in the range of 20–90 °C, the temperature coefficient of resistance (TCR) value is nearly 0.97 $\%\cdot°C^{-1}$ (Fig. S8 in the ESM). In addition, the relative current change of PCM ionic gel shows a stable rising and falling trend in three temperature deviation cycles at 20 and 60 °C in Fig. 6(c), and the maximum and minimum values remain constant at the end of each cycle. The stable and reliable electrical response signals ensure the

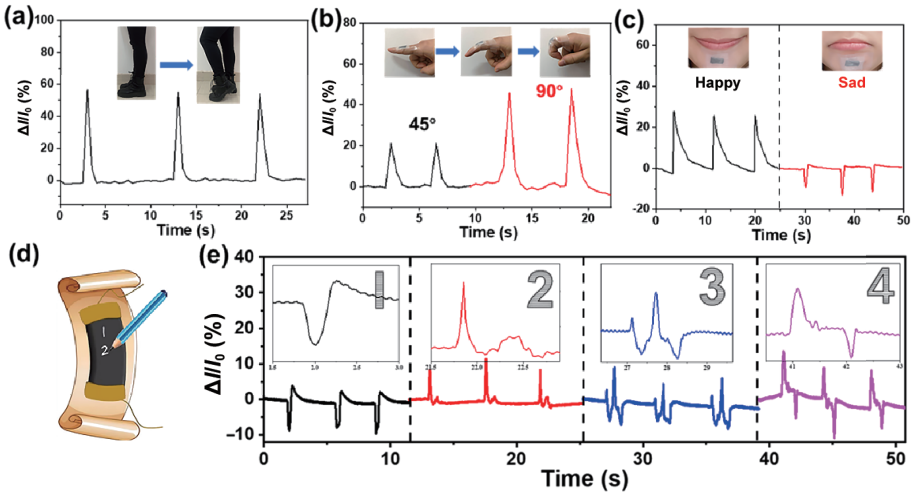

Figure 5 Relative resistance changes of strain sensors in response to (a)–(c) knee joint bending, finger bending at 45° and 90°, and facial expressions of smiling and crying. (d) Profile of the assembled smart board for writing perception. (e) The current response to Arabic number writings (20 ± 2 °C).

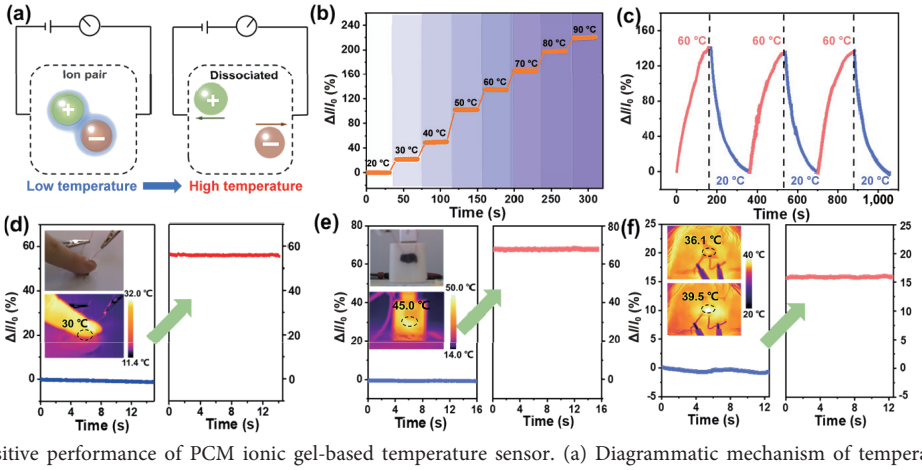

Figure 6 Thermal sensitive performance of PCM ionic gel-based temperature sensor. (a) Diagrammatic mechanism of temperature sensing. (b) The relative current changes of PCM ionic gel at different temperatures. (c) The relative current change in three temperature deviation cycles at 20 °C and 60 °C. The relative current change in response to (d)–(f) finger touching, charger heating, and simulated "artificial fever".

superior thermosensitive performance of the PCM ionic gel, prospecting its desirable approach as a temperature sensor.

Subsequently, the PCM ionic gel is assembled into a thermal indicator to explore its perception of actual ambient temperature conditions. Figure 6(d) shows the transient changes in relative current when the finger touches the sensor surface. It can be identified from the infrared thermal imaging that, after the contact of the finger, the temperature of the gel rises sharply from 11.4 to 30.0 °C, and the relative current change increases drastically to 57%. With the timely temperature perception, the gel sensor can be applied to be an overheating-alarm annunciator of the electrical apparatus. In Fig. 6(e), the gel sensor adheres to the shell surface of a mobile power source undercharging, the relative current changes by 68% as the temperature rises from 14 to 45 °C. With precise state of charge monitoring and safety assessment, the temperature sensor is expected to be a reliable component in the battery safety management system. Moreover, with high TCR sensitivity, this temperature sensor can monitor sophisticated human body temperature. Heat source approaching, i.e., thermal radiation way, is conducted to simulate human fever. As revealed in Fig. 6(f), the relative current change manifests distinct evolvement (16%) when the temperature changes from 36.1 to 39.5 °C, suggesting the promising prospect of the temperature sensor as a medical auxiliary temperature detector.

3.7 Photothermal effect and the promoted self-healing performance

Photothermal conversion is a primitive and efficient method of utilizing solar energy. With low difficulty in operation and abundant material selectivity, photothermal conversion has gained extensive research interest in the fields of power generation, water treatment, cancer treatment for decades [35–37]. Due to the photothermal property of MXene, PCM ionic gel displays excellent photothermal conversion features. The ultraviolet and visible spectra of PCM ionic gel present a wide range of absorption in the whole band and a characteristic absorption peak near 808 nm (Fig. S9(a) in the ESM). Subsequently, an 808 nm near-infrared laser is selected to carry out the following experiments.

The photothermal behavior of PCM ionic gel displays power density dependence and MXene concentration dependence in Figs. 7(a) and 7(b). Under 808 nm laser irradiation, the temperature increases rapidly to reach a maximum temperature and maintains steady afterward, showing a satisfying photothermal conversion property. Figure 7(b) indicates that the temperature change is directly proportional to the MXene content. Ultimately, the comprehensive photothermal effect of PCM ionic gel with 0.8 wt.% MXene can reach a constant temperature of 85 °C within 100 s under 808 nm laser irradiation (power density 0.6 W·cm^{-2}). Thermal images clearly show the temperature evolution of the gel during laser irradiation (Fig. S9(b) in the ESM). The MXene-based PCM ionic gel also performs excellent photothermal stability under repeated laser turn ON-OFF cycles (Fig. S9(c) in the ESM).

Based on the excellent photothermal conversion of MXene nanosheets, PCM ionic gel shows high feasibility to near-infrared

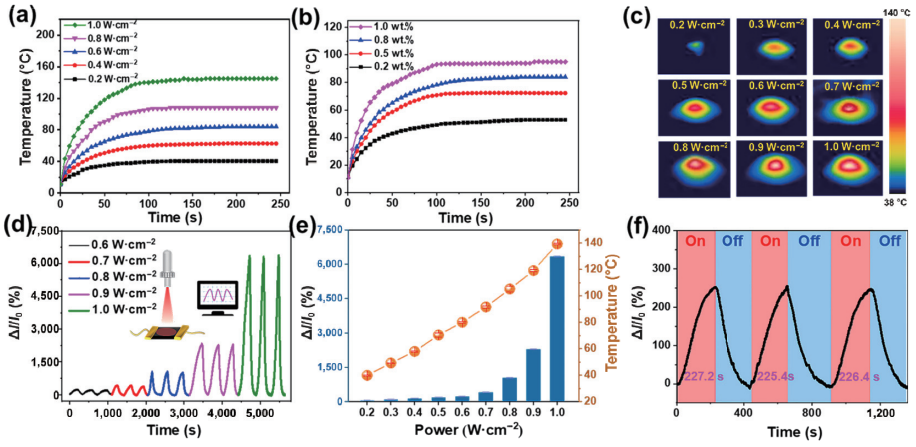

Figure 7 Electrical response of PCM ionic gels to light irradiation. (a) The temperature rise of PCM ionic at light power densities ranging from 0.2 to 1.0 W·cm^{-2}. (b) The temperature rise of PCM ionic with different MXene contents under 808 nm laser irradiation (0.6 W·cm^{-2}). (c) Thermal images under different laser power densities. (d) The relative current variations under different laser power densities (0.6, 0.7, 0.8, 0.9 and 1.0 W·cm^{-2}) for consecutive 3 cycles. (e) Summarized changes of temperature and relative current variations under different laser power densities. (f) Response time during three ON-OFF cycles.

light perception. The cuboid gel, with a dimension of 10 mm × 5 mm × 2 mm, is placed directly below the laser emitter, the distance from the laser emission point to the gel surface is arranged to be 3 cm to avoid excessive heating (Fig. S9(e) in the ESM). The PCM ionic gel shows a rapid and sensitive response to laser irradiation. In Fig. 7(d) and Fig. S9(d) in the ESM, when the laser power density increases from 0.2 to 1.0 W·cm^{-2}, the responsive $\Delta I/I_0$ rises from 57.4% to 6,333.9% with stable signal output at each cycle. The thermal images of the achievable highest temperature under different laser power densities are exhibited in Fig. 7(c). Figure 7(e) summarizes the maximum temperature and the corresponding relative current variation under different power densities laser irradiation, displaying a monotonically increasing relationship. The sensing mechanism of near-infrared light is elaborated in Fig. S10 in the ESM. With the featured photothermal effect in MXene nanosheets, the high-power-density laser irradiation stimulates a transient temperature rise. Subsequently, the heat generated transfers to the adjacent ionic liquid to accelerate the ion pair's dissociation and further facilitates rapid mobility of charge carriers to improve conductivity, and finally leads to a sharp change in the relative current. The stability and repeatability of relative current changes in consecutive laser irradiations ON-OFF cycles are analyzed in Fig. 7(f) at a laser power density of 0.6 W·cm^{-2}. The current changes are constant in three cycles with a responsive $\Delta I/I_0$ of ~ 250%, and the response time of the three rise processes is almost consistent (227.2, 225.4, and 226.4 s). The superior photothermal performance and stability promise the PCM ionic gel an excellent material for light perception.

Furthermore, the photothermal effect in PCM ionic gel also promotes a brand new concept in gel repair. The introduction of self-healing property in the gel-based sensor is a critical factor to avoid performance degradation or sudden failure under excessive external force. PCM ionic gels are equipped with self-healing features with tremendous reversible bonds in the network structure. Figure 8(e) elucidates the underlying mechanism for self-healing, where the covalent chelating bond between borax and catechol groups and widespread reversible hydrogen bonds can spontaneously recombine after a fracture. However, the polymer chains migration and recombination of polymer chains or specific reversible chemical reactions are significantly restricted under ambient temperature, showing depressed self-healing efficiency. As displayed in Fig. 8(a), the stress-strain curves of PCM ionic gels under different healing conditions are compared. The healing efficiency improves distinctly with extension in healing time and temperature. For example, the healing efficiency increases from 32.9% to 90.6 % when the healing time is prolonged from 3 to 12 h. Specifically, when the healing temperature rises to 60 °C, the healing efficiency can violently climb to 95.3% within a half-hour, achieving favorable applicability in practice.

Attributed to the satisfying photothermal effect and rapid and sensitive perception to light of PCM ionic gel, rapid and high-

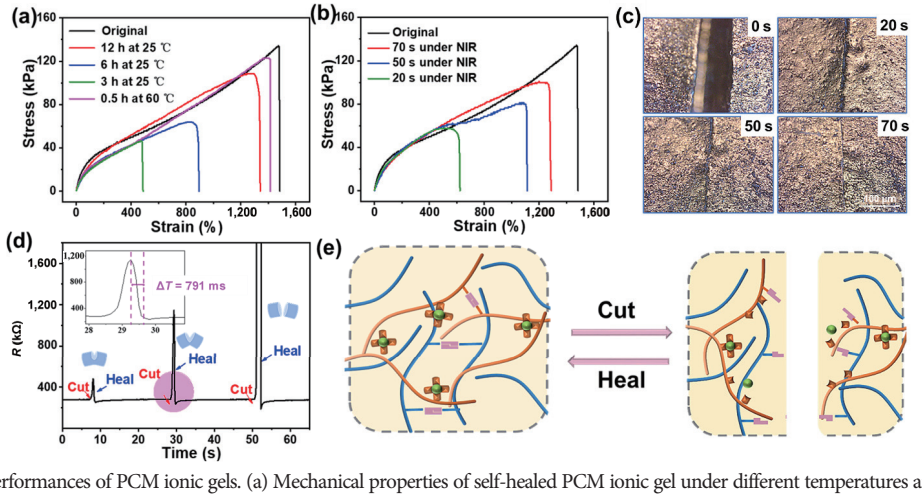

Figure 8 Self-healing performances of PCM ionic gels. (a) Mechanical properties of self-healed PCM ionic gel under different temperatures and healing time. (b) Self-healing performance under near-infrared laser irradiation. (c) Pictures of gel's surface before and after self-healing. (d) Electrical self-healable performance. (e) The schematic mechanism for self-healing property.

efficient self-healing is facile to reach under specific irradiation. 911 presents the healing profiles of PCM ionic gel after near-infrared light irradiation. PCM ionic gels maintain stretchability and conductivity after healing, showing a satisfying self-healing performance. Particularly, near-infrared light is possessed with deeper penetration depth to realize fast temperature rise at a rapid heating rate, revealing a prominent advantage over traditional thermally activated or light-induced assistance. The convenient near-infrared light irradiation also inspires self-healing at targeted damaged positions to promote localized repair. Figure 8(b) compares the stress-strain curves of the gel under 808 nm laser irradiation (0.6 $W \cdot cm^{-2}$) for different healing times. The results show that the self-healing efficiency reaches 85% after 70 s irradiation, which corroborates that the near-infrared-light irradiation can effectively accelerate the healing process and achieve a superior healing effect. Figure 8(c) manifests the morphological evolution of the incision on the gel's surface during irradiation, it is clear that the incision nearly vanishes after 70 s irradiation. Figure 8(d) displays the electrical response of the healing process under repeated cut-heal cycles. The resistance of the gel almost restores to its initial state immediately when the gel is reconnected with a certain healing time of 791 ms. It is speculated that the rapid reconstruction of dynamic bonds of the polymer network restores the contact status between MXene nanosheets and instantly repairs the ion conductive network, finally showing unattenuated electrical signals.

4 Conclusions

In summary, a facile and scalable method to prepare high-performance and high-durable ionic gels is presented. The MXene composited PCM ionic gel reveals excellent tensile property (1, 470%), superior frost/heat resistance (–50 °C/80 °C), and ultra-long mechanical durability. In combination with the electron-conductive MXene nanosheets and the ion-conductive ILs, as well as evolutional conductivity with temperature, the PCM ionic gel is successfully assembled into strain, pressure, and temperature sensors, showing sensitive perception to multiple ranges of body movements and subtle temperature variation and proposing a great potential in the fields of human-computer interaction and wearable devices. In addition, MXene nanosheets also perform strong near-infrared absorption and efficient photothermal conversion, presenting high applicability to be utilized as an optical sensor to respond to specific laser and power densities. Specifically, with distinct temperature increase under laser irradiation, the PCM ionic gels manifest marvelous self-healing promotion in both speed and effectiveness, featuring a wide prospect in practical application.

Acknowledgements

The work was supported by Jiangsu Province Policy Guidance Plan (No. BZ2019014), NSF of Jiangsu Province (No. BK20190688), NSF of the Jiangsu Higher Education Institutions (No. 21KJB430039), and 'Taishan scholars' construction special fund of Shandong Province.

Electronic Supplementary Material: Supplemental materials (Fourier-transform infrared spectroscopy spectra of CNC, TA, and CNC@TA, atomic force microscope images of CNC and CNC@TA, X-ray diffraction patterns of MXene and MAX, transmission electron microscopy image of MXene nanosheets, Cyclic stretching-releasing test, differential Scanning Calorimetry of PCM ionic gel, the response time of PCM ionic gel-based strain sensor under a subtle stretch, tensile durability test at consecutive 0–25% strain loading-uploading cycles, Electrical response of the strain sensor at temperatures of 10, 25, and 50 °C under 100% strain, electrical response of the PCM ionic gel pressure sensor, TCR of PCM ionic gel, photothermal performance of PCM ionic gel, diagram profile of the underlying mechanism for NIR optical sensing, dtretching performance of ionic gel after a cut-heal cycle, brightness changes of the small bulb during the self-healing process) is available in the online version of this article at https://doi.org/10.1007/s12274-021-4032-5.

References

[1] Kim, D. H.; Song, J. Z.; Choi, W. M.; Kim, H. S.; Kim, R. H.; Liu, Z. J.; Huang, Y. Y.; Hwang, K. C.; Zhang, Y. W.; Rogers, J. A. Materials and noncoplanar mesh designs for integrated circuits with linear elastic responses to extreme mechanical deformations. *Proc. Natl. Acad. Sci. USA* **2008**, *105*, 18675–18680.

[2] Huang, S.; Huang, Y. L.; Li, Q. Photodeformable liquid crystalline polymers containing functional additives: Toward photomanipulatable intelligent soft systems. *Small Struct.* **2021**, *2*, 2100038.

[3] Kang, K.; Park, J.; Kim, K.; Yu, K. J. Recent developments of emerging inorganic, metal and carbon-based nanomaterials for pressure sensors and their healthcare monitoring applications. *Nano Res.* **2021**, *14*, 3096–3111.

[4] Fu, X. Y.; Wang, L. L.; Zhao, L. J.; Yuan, Z. Y.; Zhang, Y. P.; Wang, D. Y.; Wang, D. P.; Li, J. Z.; Li, D. D.; Shulga, V. et al. Controlled assembly of MXene nanosheets as an electrode and active layer for high-performance electronic skin. *Adv. Funct. Mater.* **2021**, *31*, 2010533.

[5] Cai, Y. C.; Shen, J.; Dai, Z. Y.; Zang, X. X.; Dong, Q. C.; Guan, G. F.; Li, L. J.; Huang, W.; Dong, X. C. Extraordinarily stretchable all-carbon collaborative nanoarchitectures for epidermal sensors. *Adv. Mater.* **2017**, *29*, 1606411.

[6] Zhao, L. J.; Wang, L. L.; Zheng, Y. Q.; Zhao, S. F.; Wei, W.; Zhang, D. W.; Fu, X. Y.; Jiang, K.; Shen, G. Z.; Han, W. Highly-stable polymer-crosslinked 2D MXene-based flexible biocompatible electronic skins for *in vivo* biomonitoring. *Nano Energy* **2021**, *84*, 105921.

[7] Zhang, W.; Feng, P.; Chen, J.; Sun, Z. M.; Zhao, B. X. Electrically conductive hydrogels for flexible energy storage systems. *Prog. Polym. Sci.* **2019**, *88*, 220–240.

[8] Qu, X. Y.; Wang, S. Y.; Zhao, Y.; Huang, H.; Wang, Q.; Shao, J. J.; Wang, W. J.; Dong, X. C. Skin-inspired highly stretchable, tough and adhesive hydrogels for tissue-attached sensor. *Chem. Eng. J.* **2021**, *425*, 131523.

[9] Kamoun, E. A.; Kenawy, E. R. S.; Chen, X. A review on polymeric hydrogel membranes for wound dressing applications: PVA-based hydrogel dressings. *J. Adv. Res.* **2017**, *8*, 217–233.

[10] Hu, Y. G.; Zhao, T.; Zhu, P. L.; Zhang, Y.; Liang, X. W.; Sun, R.; Wong, C. P. A low-cost, printable, and stretchable strain sensor based on highly conductive elastic composites with tunable sensitivity for human motion monitoring. *Nano Res.* **2018**, *11*, 1938–1955.

[11] Huang, J. R.; Peng, S. J.; Gu, J. F.; Chen, G. Q.; Gao, J. H.; Zhang, J.; Hou, L. X.; Yang, X. X.; Jiang, X. C.; Guan, L. H. Self-powered integrated system of a strain sensor and flexible all-solid-state supercapacitor by using a high performance ionic organohydrogel. *Mater. Horiz.* **2020**, *7*, 2085–2096.

[12] Xu, J. J.; Jing, R. N.; Ren, X. Y.; Gao, G. H. Fish-inspired anti-icing hydrogel sensors with low-temperature adhesion and toughness. *J. Mater. Chem. A* **2020**, *8*, 9373–9381.

[13] Ge, G.; Lu, Y.; Qu, X. Y.; Zhao, W.; Ren, Y. F.; Wang, W. J.; Wang, Q.; Huang, W.; Dong, X. C. Muscle-inspired self-healing hydrogels for strain and temperature sensor. *ACS Nano* **2020**, *14*, 218–228.

[14] Zhang, X. F.; Ma, X. F.; Hou, T.; Guo, K. C.; Yin, J. Y.; Wang, Z. G.; Shu, L.; He, M.; Yao, J. F. Inorganic salts induce thermally reversible and anti-freezing cellulose hydrogels. *Angew. Chem., Int. Ed.* **2019**, *58*, 7366–7370.

[15] Zhang, H. X.; Niu, W. B.; Zhang, S. F. Extremely stretchable, stable,

and durable strain sensors based on double-network organogels. *ACS Appl. Mater. Interfaces* **2018**, *10*, 32640–32648.

[16] Han, S. J.; Liu, C. R.; Lin, X. Y.; Zheng, J. W.; Wu, J.; Liu, C. Dual conductive network hydrogel for a highly conductive, self-healing, anti-freezing, and non-drying strain sensor. *ACS Appl. Polym. Mater.* **2020**, *2*, 996–1005.

[17] Yu, Q. Y.; Qin, Z. H.; Ji, F.; Chen, S.; Luo, S. Y.; Yao, M. M.; Wu, X. J.; Liu, W. W.; Sun, X.; Zhang, H. T. et al. Low-temperature tolerant strain sensors based on triple crosslinked organohydrogels with ultrastretchability. *Chem. Eng. J.* **2021**, *404*, 126559.

[18] Zhang, Y. W.; Yuan, B.; Zhang, Y. Q.; Cao, Q. P.; Yang, C.; Li, Y.; Zhou, J. H. Biomimetic lignin/poly(ionic liquids) composite hydrogel dressing with excellent mechanical strength, self-healing properties, and reusability. *Chem. Eng. J.* **2020**, *400*, 125984.

[19] Zhang, Y. C.; Li, M. X.; Qin, B.; Chen, L. L.; Liu, Y. C.; Zhang, X.; Wang, C. Highly transparent, underwater self-healing, and ionic conductive elastomer based on multivalent ion-dipole interactions. *Chem. Mater.* **2020**, *32*, 6310–6317.

[20] Li, T. Q.; Wang, Y. T.; Li, S. H.; Liu, X. K.; Sun, J. Q. Mechanically robust, elastic, and healable ionogels for highly sensitive ultra-durable ionic skins. *Adv. Mater.* **2020**, *32*, 2002706.

[21] Zhao, G. R.; Zhang, Y. W.; Shi, N.; Liu, Z. R.; Zhang, X. D.; Wu, M. Q.; Pan, C. F.; Liu, H. L.; Li, L. L.; Wang, Z. L. Transparent and stretchable triboelectric nanogenerator for self-powered tactile sensing. *Nano Energy* **2019**, *59*, 302–310.

[22] Zhao, X. L.; Zhou, K. L.; Zhong, Y. J.; Liu, P.; Li, Z. C.; Pan, J. L.; Long, Y.; Huang, M. R.; Brakat, A.; Zhu, H. W. Hydrophobic ionic liquid-in-polymer composites for ultrafast, linear response and highly sensitive humidity sensing. *Nano Res.* **2021**, *14*, 1202–1209.

[23] Ghatee, M. H.; Zare, M.; Moosavi, F.; Zolghadr, A. R. Temperature-dependent density and viscosity of the ionic liquids 1-alkyl-3-methylimidazolium iodides: Experiment and molecular dynamics simulation. *J. Chem. Eng. Data* **2010**, *55*, 3084–3088.

[24] Ota, H.; Chen, K.; Lin, Y. J.; Kiriya, D.; Shiraki, H.; Yu, Z. B.; Ha, T. J.; Javey, A. Highly deformable liquid-state heterojunction sensors. *Nat. Commun.* **2014**, *5*, 5032.

[25] Gui, Q. Y.; He, Y. L.; Gao, N. W.; Tao, X. L.; Wang, Y. P. A skin-inspired integrated sensor for synchronous monitoring of multiparameter signals. *Adv. Funct. Mater.* **2017**, *27*, 1702050.

[26] Kang, J.; Tok, J. B. H.; Bao, Z. N. Self-healing soft electronics. *Nat. Electron.* **2019**, *2*, 144–150.

[27] Ge, G.; Yuan, W.; Zhao, W.; Lu, Y.; Zhang, Y. Z.; Wang, W. J.; Chen, P.; Huang, W.; Si, W. L.; Dong, X. C. Highly stretchable and autonomously healable epidermal sensor based on multi-functional hydrogel frameworks. *J. Mater. Chem. A* **2019**, *7*, 5949–5956.

[28] Zhao, L.; Ren, Z. J.; Liu, X.; Ling, Q. J.; Li, Z. J.; Gu, H. B. A multifunctional, self-healing, self-adhesive, and conductive sodium alginate/poly(vinyl alcohol) composite hydrogel as a flexible strain sensor. *ACS Appl. Mater. Interfaces* **2021**, *13*, 11344–11355.

[29] Chen, J. S.; Peng, Q. Y.; Thundat, T.; Zeng, H. B. Stretchable, injectable and self-healing conductive hydrogel enabled by multiple hydrogen bonding toward wearable electronics. *Chem. Mater.* **2019**, *31*, 4553–4563.

[30] Zhao, W.; Qu, X. Y.; Xu, Q.; Lu, Y.; Yuan, W.; Wang, W. J.; Wang, Q.; Huang, W.; Dong, X. C. Ultrastretchable, self-healable, and wearable epidermal sensors based on ultralong Ag nanowires composited binary-networked hydrogels. *Adv. Electron. Mater.* **2020**, *6*, 2000267.

[31] Pena-Francesch, A.; Jung, H.; Demirel, M. C.; Sitti, M. Biosynthetic self-healing materials for soft machines. *Nat. Mater.* **2020**, *19*, 1230–1235.

[32] Wang, K.; Lou, Z.; Wang, L. L.; Zhao, L. J.; Zhao, S. F.; Wang, D. Y.; Han, W.; Jiang, K.; Shen, G. Z. Bioinspired interlocked structure-induced high deformability for two-dimensional titanium carbide (MXene)/natural microcapsule-based flexible pressure sensors. *ACS Nano* **2019**, *13*, 9139–9147.

[33] Wang, D. Y.; Wang, L. L.; Lou, Z.; Zheng, Y. Q.; Wang, K.; Zhao, L. J.; Han, W.; Jiang, K.; Shen, G. Z. Biomimetic, biocompatible and robust silk Fibroin-MXene film with stable 3D cross-link structure for flexible pressure sensors. *Nano Energy* **2020**, *78*, 105252.

[34] Cai, Y. C.; Shen, J.; Ge, G.; Zhang, Y. Z.; Jin, W. Q.; Huang, W.; Shao, J. J.; Yang, J.; Dong, X. C. Stretchable $Ti_3C_2T_x$ MXene/carbon nanotube composite based strain sensor with ultrahigh sensitivity and tunable sensing range. *ACS Nano* **2018**, *12*, 56–62.

[35] Li, R. Y.; Zhang, L. B.; Shi, L.; Wang, P. MXene Ti_3C_2: An effective 2D light-to-heat conversion material. *ACS Nano* **2017**, *11*, 3752–3759.

[36] Xing, C. Y.; Chen, S. Y.; Liang, X.; Liu, Q.; Qu, M. M.; Zou, Q. S.; Li, J. H.; Tan, H.; Liu, L. P.; Fan, D. Y. et al. Two-dimensional MXene (Ti_3C_2) integrated cellulose hydrogels: Toward smart three-dimensional network nanoplatforms exhibiting light-induced swelling and bimodal photothermal/chemotherapy anticancer activity. *ACS Appl. Mater. Interfaces* **2018**, *10*, 27631–27643.

[37] Xu, X. W.; Chen, Y. C.; He, P.; Wang, S.; Ling, K.; Liu, L. H.; Lei, P. F.; Huang, X. J.; Zhao, H.; Cao, J. Y. et al. Wearable CNT/$Ti_3C_2T_x$ MXene/PDMS composite strain sensor with enhanced stability for real-time human healthcare monitoring. *Nano Res.* **2021**, *14*, 2875–2883.

[38] Liu, G. Y.; Zou, J. H.; Tang, Q. Y.; Yang, X. Y.; Zhang, Y. W.; Zhang, Q.; Huang, W.; Chen, P.; Shao, J. J.; Dong, X. C. Surface modified Ti_3C_2 MXene nanosheets for tumor targeting photothermal/photodynamic/chemo synergistic therapy. *ACS Appl. Mater. Interfaces* **2017**, *9*, 40077–40086.

[39] Yuan, W.; Qu, X. Y.; Lu, Y.; Zhao, W.; Ren, Y. F.; Wang, Q.; Wang, W. J.; Dong, X. C. MXene-composited highly stretchable, sensitive and durable hydrogel for flexible strain sensors. *Chin. Chem. Lett.* **2021**, *32*, 2021–2026.

[40] Calver, P. Hydrogels for soft machines. *Adv. Mater.* **2009**, *21*, 743–756.

[41] Simha, N. K.; Carlson, C. S.; Lewis, J. L. Evaluation of fracture toughness of cartilage by micropenetration. *J. Mater. Sci. Mater. Med.* **2004**, *15*, 631–639.

[42] Shao, C. Y.; Wang, M.; Meng, L.; Chang, H. L.; Wang, B.; Xu, F.; Yang, J.; Wan, P. B. Mussel-inspired cellulose nanocomposite tough hydrogels with synergistic self-healing, adhesive, and strain-sensitive properties. *Chem. Mater.* **2018**, *30*, 3110–3121.

[43] Shao, C. Y.; Meng, L.; Wang, M.; Cui, C.; Wang, B.; Han, C. R.; Xu, F.; Yang, J. Mimicking dynamic adhesiveness and strain-stiffening behavior of biological tissues in tough and self-healable cellulose nanocomposite hydrogels. *ACS Appl. Mater. Interfaces* **2019**, *11*, 5885–5895.

[44] Ding, Y.; Zhang, J. J.; Chang, L.; Zhang, X. Q.; Liu, H. L.; Jiang, L. Preparation of high-performance ionogels with excellent transparency, good mechanical strength, and high conductivity. *Adv. Mater.* **2017**, *29*, 1704253.

[45] Lu, Y.; Qu, X. Y.; Zhao, W.; Ren, Y. F.; Si, W. L.; Wang, W. J.; Wang, Q.; Huang, W.; Dong, X. C. Highly stretchable, elastic, and sensitive MXene-based hydrogel for flexible strain and pressure sensors. *Research* **2020**, *2020*, 2038560.

[46] Tan, J. Y.; Li, S. S.; Liu, B. L.; Cheng, H. M. Structure, preparation, and applications of 2D material-based metal-semiconductor heterostructures. *Small Struct.* **2021**, *2*, 2170001.